BIOLOGY, MEDICINE, & NATURAL PRODUCT CHEMISTRY ISSN 2089-6514 (paper)
Volume 15, Number 1, April 2026 | Pages: 739-748 | DOI: 10.14421/biomedich.2026.151.739-748 ISSN 2540-9328 (online)

Isolation of Secondary Metabolites from the Antioxidant Active Fraction of *Syzygium aqueum* Leaves and Its Docking Simulation on EGFR

Farid Algani, Afrizal Itam*, Mai Efdi, Kuntum Suci Mawarni
Chemistry Department, Faculty of Mathematics and Natural Sciences, Andalas University,
Jl. Limau Manis, Sumatera Barat 25163, Tel. +62-751-71181, Fax. +62-751-71085, Indonesia.

Corresponding author*
afrizalitam@sci.unand.ac.id

Manuscript received: 18 November 2025. Revision accepted: 06 May 2026, Published: 31 May 2026.

Abstract

This study aims to isolate secondary metabolites from *Syzygium aqueum* leaves and assess their suitability for targeting Epidermal Growth Factor Receptor (EGFR) proteins in lung cancer treatment. The methods utilized include maceration, fractionation, chromatography, and molecular docking. The isolated compounds were characterized using UV-VIS spectroscopy, FTIR, and NMR techniques. The compounds were 2',4'-dihydroxy-6'-methoxy-3',5'-dimethylchalcone (DMC) and lupeol. Molecular docking simulations were performed between DMC compounds and EGFR proteins (PDB ID: 1M17, 5D41, 5UG8, 5UG9, and 6LUD). Mutations in the EGFR kinase domain, particularly T790M, L858R, and V948R, confer resistance to first-generation inhibitors, including osimertinib. According to the in-silico docking results, DMC shows promise as an alternative inhibitor candidate. It can maintain interactions with the key residue Lys745 and provides stabilization through Asp855 ansamod Glu762. In contrast, osimertinib relies more on hydrophobic interactions and loses direct contact with Lys745, contributing to decreased affinity. This suggests that DMC may effectively overcome resistance associated with mutations, especially T790M, while maintaining crucial interactions within the ATP binding pocket. Therefore, DMC can be developed into a new non-covalent scaffold for treating lung cancer with EGFR mutations.

Keywords: *Syzygium aqueum*; Isolation; 2',4'-dihydroxy-6'-methoxy-3',5'-dimethylchalcone (DMC); Molecular docking; Lung cancer.

INTRODUCTION

The *Syzygium aqueum* is a plant native to Indonesia, primarily found on the island of Java (Manaharan et al. 2012). It is commonly utilized in traditional medicine to treat bacterial infections, alleviate itching, reduce swelling, and address conditions like a cracked tongue (Habisukan et al. 2021) (Osman et al. 2009). This plant has demonstrated several pharmacological properties, including antidiabetic, anti-inflammatory, antioxidant, hepatoprotective, antimicrobial, and anticancer effects (Chandana et al. 2024). 2′,4′-Dihydroxy-6′-methoxy-3′,5′-dimethylchalcone (DMC) is one of the bioactive compounds isolated from *S. aqueum* that possesses notable antioxidant activity(Ei Ei Aung et al. 2020). It protects the body's cells from oxidative damage caused by free radicals, whose excessive accumulation can lead to degenerative diseases such as cardiovascular and cerebrovascular disorders, as well as cancer (Lee et al. 2003). DMC showed significant antiproliferative activity against A549 lung cancer cells, while inducing apoptosis via activation of caspase-9 and caspase-3 (Hadisaputri et al. 2020).

Lung cancer is one of the most deadly diseases in the world. It occurs when normal cells undergo mutations, leading to uncontrolled growth (Khamto et al. 2021). One of the most common treatments for cancer is chemotherapy; however, it can cause significant damage to normal cells (Hadisaputri et al. 2020). In the case of lung cancer, chemotherapy works by inhibiting the activity of the Epidermal Growth Factor Receptor (EGFR) (Khuswatun Khazanah Ishak and Yuliana 2024). EGFR is a receptor protein that plays a crucial role in cell proliferation, angiogenesis, metastasis, and the inhibition of the apoptosis process. When EGFR is overexpressed, it can promote cancer cell growth. Tyrosine Kinase Inhibitors (TKIs) are designed to inhibit EGFR expression by disrupting the protein kinase signal transduction pathway (Rasyid, Purwono, and Pranowo 2021). These small molecules function by breaking down adenosine triphosphate (ATP) bonds within the intracellular tyrosine kinase region, leading to tumor regression through increased apoptosis, reduced cellular proliferation, and decreased angiogenesis (Khuswatun Khazanah Ishak and Yuliana 2024). Several generations of TKIs targeting EGFR mutations have been developed. Erlotinib and gefitinib are first-generation of TKIs that target EGFR and effectively suppress cancer cell proliferation. However, resistance commonly emerges within about two years, ultimately diminishing their

long-term therapeutic efficacy (Rasyid, Purwono, and Pranowo 2021). To overcome this limitation, second-generation EGFR inhibitors such as afatinib and dacomitinib were developed, which target multiple forms of EGFR including the wild type, although their activity may lead to increased side effects (Khuswatun Khazanah Ishak and Yuliana 2024). To address the limitations of earlier generations, third-generation TKIs such as osimertinib were developed, exhibiting approximately 30 to 100 fold greater activity against the EGFR T790M mutation. However, resistance may also arise from a substitution of cysteine with serine at position 797 (Rasyid, Purwono, and Pranowo 2021). Given these challenges, further research and development of anticancer agents with minimal side effects. This study aimed to isolate secondary metabolites from the leaves of *S. aqueum* and evaluate its activity against lung cancer.

MATERIALS AND METHODS

Extraction and fractionation

S. aqueum leaves weighing up to 10 kg were collected in Padang City, West Sumatra Province. These were dried and ground using a grinder. A total of 3.5 kg of ground leaves was macerated using methanol (E. E. Aung et al. 2021). The concentrated methanol extract was suspended using 500 mL of water and fractionated using hexane solvent in a 1:1 ratio. This process is carried out until the hexane fraction obtained is clear. Furthermore, it was fractionated using ethyl acetate similarly (Abdullahi R and Haque 2020).

Determination of Total Phenolic Content

The determination of total phenolics was performed on hexane, ethyl acetate, and residue fractions using the Folin-Ciocalteu method (Itam et al. 2021). A total of 1 mg of the sample was dissolved in methanol in a 10 mL volumetric flask. Then, 0.5 mL of this sample solution was transferred into a new 10 mL volumetric flask, followed by the addition of 0.5 mL of Folin–Ciocalteu reagent. The mixture was subsequently incubated for 5 minutes. After incubation, 1 mL of a 20% sodium carbonate solution was added, and the mixture was diluted with distilled water up to the mark on the flask. It was then incubated for an 2 hours. After the incubation period, the absorbance of the Mixtures was measured using a UV-Vis spectrometer at 765 nm. The total phenolic content was calculated based on a calibration curve created with gallic acid at various concentrations, reported as gallic acid equivalents per 10 mg of concentrated extract.

Determination of Total Flavonoids Content

Determination of total flavonoid content was carried out on hexane, ethyl acetate, and residue fractions using the $AlCl_3$ method (Ghafar et al. 2017). An amount 3 mg of the sample was dissolved in methanol in a 10 mL volumetric flask. Subsequently, 1 mL of sample solution was put into a 10 mL volumetric flask, and than 4 mL of distilled water, and 0.3 mL of $NaNO_2$ solution were added, then incubated for 5 minutes. Furthermore, 0.3 mL of 10% $AlCl_3$ solution was added and incubated for 5 minutes. After the incubation, 2 mL of 1 M NaOH solution was added to the volumetric flask, then diluted with distilled water to the limit mark. Absorbance measurements were taken at a wavelength of 510 nm using a UV-Vis spectrophotometer. Total flavonoid content was calculated based on the calibration curve of 5 quercetins at various concentrations, and expressed as quercetin equivalents per 10 mg of concentrated extract.

Determination of antioxidant

Antioxidant activity was carried out on hexane, ethyl acetate, and residue fractions using the DPPH free radical scavenging method (Itam et al. 2021). The negative control was methanol, while the positive was ascorbic acid. Parent solution with a concentration of 1,000 µg/mL was made by dissolving 10 mg of the sample into a 10 mL volumetric flask. Furthermore, concentration variations were made: 300, 400, 500, 600, 700, and 800 µg/mL for the hexane fraction, and 5, 10, 20, 30, 40, and 50 µg/mL for the ethyl acetate fraction and the residual fraction. Each concentration variation and control was put into a vial as a volume of 1 mL, then 3 mL of DPPH solution was added. The mixture was incubated for 30 minutes in a dark room. Absorbance was measured using a UV-Vis spectrophotometer at a wavelength of 517 nm. Based on the absorbance values obtained, the percentage (%) of inhibition was calculated using the following formula:

$$\%\ Inhibiton = \frac{Absorbance\ control - Absorbance\ Sample}{Absorbance\ control} \times 100 \quad (1)$$

The percentage inhibition (% Inhibition) was determined according to Equation (1), with Absorbance control referring to the control absorbance and Absorbance sample representing the absorbance of the extract.

Isolation of Secondary Metabolite Compound

Isolation of secondary metabolite compounds was conducted on the ethyl acetate fraction. The preliminary layer chromatography (TLC) test was carried out by dissolving the sample, then spotting it on a TLC plate and eluting using hexane and ethyl acetate eluent with a ratio of 8:2. The TLC results were observed under UV light to determine the elution method used in column chromatography (Efdi 2024). Isolation by column chromatography was performed using hexane and ethyl acetate eluents. The eluate was tested using TLC to see the stain separation pattern. The eluate with the same stain pattern was combined in a vial bottle. From several fractions obtained, fractions with simple stain patterns or single stains were selected for further purification.

Purification of isolated compounds was carried out by column chromatography for compound 1 and the trituration method for compound 2 (Zala et al. 2012). The purification was tested using TLC with a mixture of hexanes and ethyl acetate eluents, in the ratios of 9:1, 8.5:1.5, and 8:2 for compound 1 and 9.5:0.5, 9:1, 8.5:1.5 for compound 2.

Characterization of Secondary Metabolite Compounds

The isolated compounds were analyzed by UV-Vis, FTIR, and NMR.

Molecular Docking of isolated compounds to EGFR target proteins

Compound 1 was evaluated against EGFR proteins (PDB ID 1M17, 5D41, 5UG8, 5UG9, and 6LUD) and compared with osimertinib. The proteins were downloaded in pdb format from https://www.rcsb.org/, while the 3D structures of compound 1 and osimertinib were downloaded from the PubChem website in SDF format, then converted to pdb format via https://cactus.nci.nih.gov/translate/ (National Cancer Institute). The separation of receptors and natural ligands from EGFR proteins was performed using Pymol in pdbqt format. The preparation of receptors and ligands was performed using AutoDockTools, followed by the docking process. The 2D interaction between ligands and amino acid residues from EGFR proteins was visualized using Discovery Studio Visualizer software (Wang et al. 2021).

RESULTS AND DISCUSSION

Extraction and fractionation

A concentrated methanol extract weighing 530 g was obtained from *S. aqueum* leaves. A total of 260 g were fractionated from this extract using hexane and ethyl acetate solvents. The yields of the fractions were as follows: the yield of hexane fraction was 24 g (9% yield), 29 g of ethyl acetate fraction (18.85% yield), and 160 g of residue fraction (61.54% yield).

Determination of Total Phenolic Content

The total phenolic content was measured using a gallic acid standard, with the regression equation represented as $y = 0.0046x + 0.0135$ ($R^2 = 0.9959$), as illustrated in Figure 1. The calculated total phenolic contents for the hexane, ethyl acetate, and residue fractions were 212 mg, 451.1 mg, and 307.6 mg of gallic acid equivalents per gram (GAE/g), respectively. This data indicates that phenolic compounds were most abundant in the ethyl acetate fraction, followed by the residue fraction, and then the hexane fraction.

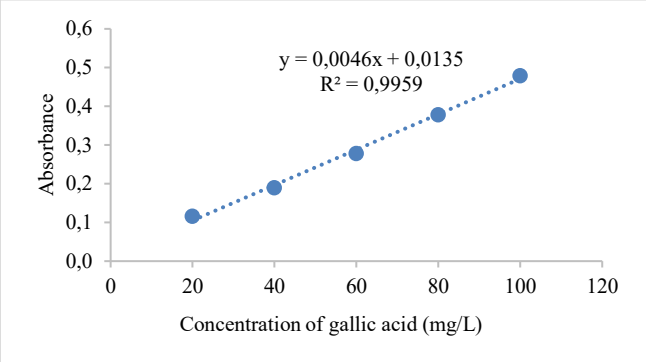

Figure 1. Standard solution curve of gallic acid.

Determination of Total Flavonoids Content

The standard used to determine the total flavonoid content is quercetin, represented by the regression equation $y = 0.0005x + 0.0441$ ($R^2 = 0.9839$), as shown in Figure 2. The total flavonoid content for the hexane, ethyl acetate, and residue fractions calculated using the quercetin calibration curve, was 46 mg, 209.4 mg, and 155.4 mg QE/g, respectively. This indicates that the ethyl acetate fraction contains the highest concentration of flavonoid compounds, followed by the residue fraction and then the hexane fraction.

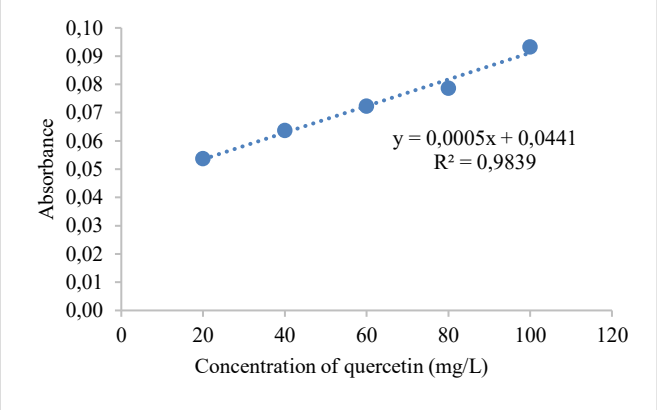

Figure 2. Standard solution curve for quercetin.

Determination of Antioxidants

Samples that contain antioxidant compounds exhibit a color change in DPPH (1,1-Diphenyl-2-picrylhydrazyl). When these antioxidant compounds neutralize the unpaired electrons in DPPH, the color shifts from purple to yellow. The intensity of the yellow color indicates the strength of the antioxidant activity; the more potent the antioxidant, the more vivid the yellow becomes. The results of the antioxidant activity measurements are presented in the table below.

Table 1. Antioxidant activity of *S. aqueum* leaf fractions.

Fraction	IC_{50} (µg/mL)	Antioxidant Activity
Hexane	469.01	Weak
Ethyl acetate	10.11	Very Strong
Residual	84.49	Strong
Ascorbic acid	3.60	Very Strong

The table indicates that the ethyl acetate fraction exhibits vigorous antioxidant activity (Jun et al. 2003) (Mustarichie, Runadi, and Ramdhani 2017). This is attributed to ethyl acetate's ability to dissolve semi-polar to polar compounds, including phenoslic and flavonoid compounds. The results of the total phenolic and total flavonoid content assays support this.

Isolation of Secondary Metabolite Compounds

Separation of compounds from the ethyl acetate fraction was conducted using column chromatography with a Step Gradient Polarity (SGP) eluent system. The eluents employed were a mixture of hexane and ethyl acetate in ratios ranging from 10:0 to 10:10. The eluate was collected in vials and analyzed using thin-layer chromatography (TLC). Based on the TLC results, the eluates that displayed similar spot patterns were combined, resulting in 11 fractions. Fractions F_4 and F_5 were then further purified using gravity column chromatography, again employing the SGP elution system. Separation of compounds in fraction F_4 was conducted using hexane and ethyl acetate eluents in ratios ranging from 10:0 to 7:3. This process resulted in five subfractions. Subfraction $F_{4.4}$ yielded the first pure compound, which had a mass of 21 mg. The second pure compound, obtained from subfraction $F_{4.2}$, was purified using the trituration method and had a mass of 48 mg. The purity of both isolated compounds was analyzed using TLC with three different eluent ratios. The first isolated compound was tested using hexane and ethyl acetate in the ratios of 9:1, 8.5:1.5, and 8:2. The second isolated compound was analyzed using the same solvents in the ratios of 9.5:0.5, 9:1, and 8.5:0.5. Based on the purity tests, it can be concluded that both isolated compounds are pure, as each one produced a single spot on the TLC plates.

The separation of compounds from fraction F_5 was achieved using hexane and ethyl acetate eluents in a ratio varying from 10:0 to 7:3, resulting in the collection of five subfractions. Subfraction $F_{5,4}$ underwent purification through gravity column chromatography with an isocratic eluent system. TLC analyses indicated that the isolated compound from subfraction $F_{5,4}$ was identical to the compound found in subfraction $F_{4,4.}$ The structure of the isolated compound was further analyzed using UV-Vis, FT-IR, and NMR spectroscopy. The structure of the first compound is illustrated in Figure 3, while the second compound is shown in Figure 4.

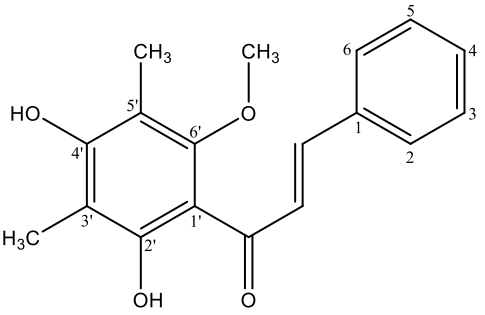

Figure 3. Structure of 2′,4′-Dihydroxy-6′-methoxy-3′,5′-dimethylchalcone (DMC).

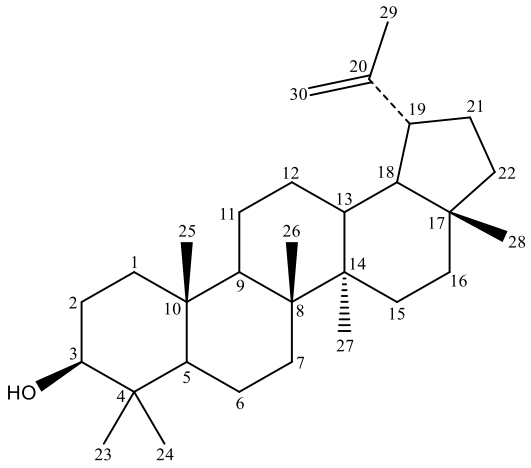

Figure 4. Structure of lupeol.

Structural Elucidation

Compound I: Yellow powder, UV-Vis λ 336.0 nm, IR ν max 3341.80, 2926, 1722,72, 1607,14 cm^{-1}; 1H NMR (400 MHz, $CDCl_3$, δ, ppm): 7.65 (2H, dd, J = 1.77 and 7.78 Hz, *H*-2), 7.40 (3H, m, *H*-4), 7.84 (1H, d, J = 15.66 Hz, *H*-β), 7.99 (1H, d, J = 15.66 Hz, *H*-α), 13.60 (1H, s, *H*-2'OH), 5.45 ppm (1H, s, *H*-4'OH), 2.14 ppm (3H, d, J = 15.88 Hz, *H*-5'CH3). ^{13}C NMR (100 MHz, $CDCl_3$): δ 135.5 (*C*-1), 130.2 (*C*-4), 128.4 (*C*-5), 128.9 (*C*-6), 142.9 (*C*-β), 126.7 (*C*-α), 193.4 (C-C=0), 106.6 (*C*-1), 162.1 (*C*-2'), 108.9 (*C*-3'), 159.2 (*C*-4'), 109.0 (*C*-5'), 158.9 (*C*-6;), 8.3 (*C*-3'CH_3), 7.6 (*C*-5'CH_3), 62.3 (*C*-6'OCH_3). Based on NMR data and literature studies, compound 1 is 2′,4′-Dihydroxy-6′-methoxy-3′,5′-dimethylchalcone. Comparison of NMR data with previously reported 2′,4′-Dihydroxy-6′-methoxy-3′,5′-dimethylchalcone can be seen in **Table 2.**

Table 2. Comparison of NMR spectrum identification of compound 1 with the literature (Vachiraarunwong et al. 2023).

Position (C)	δH (Mult, J in Hz)	δH (lit.) (Mult, J in Hz	δC (ppm)	δC (lit.) (ppm)
1	-	-	135.4	135.5
2	7.65 (dd, 1.77, 7.78)	7.64 (m)		128.9
3		7.41 (m)		128.4
4	7.40 (m)	7.41 (m)	130.2	130.2
5	-	-	128.4	128.4
6		7.54 (m)	128.9	128.9
β	7.84 (d, 15.66)	7.84 (d, 15.7)	142.9	142.9
α	7.99 (d, 15.66)	7.99 (d, 15.7)	126.7	126.7
C=O	-	-	193.4	193.4
1’	-	-	106.6	106.6
2’	-	-	162,1	162.0
3’	-	-	108.9	109.0
4’	-	-	159.2	159.3
5’	-	-	109.0	109.0
6’	-	-	158.9	158.8
2’-OH	13.60 (s)	13.69 (s)	-	-
3’-CH_3		2.14 (s)	8.3	8.2
4’-OH	5.45 (s)	5.38 (s)	-	-
5’-CH_3	2.14 (d, 15.88)	2.16 (s)	7.6	7.6
6’-OCH_3	3.66	3.66 (s)	62.4	62.3

Compound II: White crystal, UV-Vis λ 297.0 nm, IR ν max 2925.64, 1455.21, 1378 cm^{-1}; 1H NMR (400 MHz, $CDCl_3$, δ, ppm): 1.56 (1H, s, *H*-2), 1.66 (1H, s, *H*-2), 3.18 (1H, dd, J = 3.5 and 4.71 Hz, *H*-3), 0.68 (1H, s, *H*-5), 1.36 (2H, m, *H*-6), 1.25 (1H, s, *H*-9), 1.23 (2H, m, *H*-11), 1.07 (2H, m, *H*-12), 2.38 (1H, d, J = 5.87 and 11.09 Hz, *H*-19), 0.76 (1H, s, *H*-24), 0.83 (1H, s, *H*-25), 0.96 (1H, s, *H*-27), 4.69 (3H, d, J = 2.52 Hz, *H*-29), 1.92 (2H, m, *H*-30). ^{13}C NMR (100 MHz, $CDCl_3$): δ 37.8 (*C*-1), 27.4 (*C*-2), 79.0 (*C*-3), 38.9 (*C*-4), 55.3 (*C*-5), 18.3 (*C*-6), 34.3 (*C*-7), 40.8 (*C*-8), 50.4 (*C*-9), 37.2 (*C*-10), 21.0 (*C*-11), 25.1 (*C*-12), 38.1 (*C*-13), 42.8 (*C*-14), 27.4 (*C*-15), 35.6 (*C*-16), 43.0 (*C*-17), 48.0 (*C*-18), 48.3 (*C*-19), 150.9 (*C*-20), 29.9 (*C*-21), 40.0 (*C*-22), 28.0 (*C*-23), 15.4 (*C*-24), 16.1 (*C*-25), 16.0 (*C*-26), 14.6 (*C*-27), 18.0 (*C*-28), 19.3 (*C*-29), 109.3 (*C*-30). Based on NMR data and literature studies, compound 2 is lupeol. Comparison of NMR data with previously reported lupeol compounds can be seen in **Table 3.**

Table 3. Comparison of NMR spectrum identification of compound 2 with the literature (Al-Temimi and Kadhum 2023).

Position (C)	δH (Mult, J in Hz)	δH (lit.) (Mult, J in Hz	δC (ppm)	δC (lit.) (ppm)
1		Ha = 0.9 (s) Hb = 1.77 (o)	37.8	37.8
2	1.56 1.66	Ha = 1.53 (s), Hb = 1.64 (o)	27.4	27.5
3	3.18 (dd, J=4.71, 11.59 Hz)	3.33 (dd, J = 3.5, 1.8 Hz)	79.0	79,0
4		-	38.9	38.9
5	0.68 (s)	H = 0.66 (S)	55.3	55,3
6	1.36 (m)	H = 1.35 (O)	18.3	18.3
7		1.44	34.3	34.3
8		-	40.8	40.9
9	1.25 (s)	1.28 (s)	50.4	50,5
10		-	37.2	37.2
11	1.23 (m)	1.23	21.0	21.0
12	1.07 (m)	1.04 (o)	25.1	25.2
13		1.64 (o)	38.1	38.1
14		-	42.8	42.9
15		1.04 (o)	27.4	27.5
16		1.34 (o)	35.6	35.6

Position (C)	δH (Mult, J in Hz)	δH (lit.) (Mult, J in Hz	δC (ppm)	δC (lit.) (ppm)
17		-	43.0	43.0
18		1.35 (o)	48.0	48.0
19	2.38 (d, J= 5.87, 11.09 Hz)	2.3 (d, J = 11.8 Hz)	48.3	48.3
20		-	150.9	150.9
21		1.28	29.9	29.9
22		1.15 (s)	40.0	40.0
23		0.9 (s)	28.0	28.0
24	0.76 (s)	0.76 (s)	15.4	15.3
25	0.83 (s)	0.83 (s)	16.1	16.1
26		1.04 (o)	16.0	16.0
27	0.96 (m)	0.92 (s)	14.6	14.6
28		0.86 (s)	18.0	18.0
29	4.69 (d, = 2.52 Hz)	Ha:4.68 (d, J=56.0 Hz), Hb:1.77 (o)	19.3	19.3
30	1.92 (0)	1.77 (o)	109.3	109.3

Molecular Docking

Docking simulations were conducted to evaluate the potential of DMC compounds and to compare their interactions with osimertinib in both wild-type and mutated EGFR. The aim of this simulation was to predict the optimal binding locations and affinities of the ligands with the protein receptors (Ahmad et al. 2022). The results of the docking data are presented in Table 4 and the 2D visualizations can be seen in Figure 5.

Table 4. Docking data of DMC compounds with various EGFR proteins.

PDB ID	EGFR mutation	Ligand	Affinity (kkal/mol)	RMSD (Å)	Interactions
1M17	Wild type	AQ4	-7.0	0.990	**DMC:** Leu, Val, Ala, Phe, Lys Met. **Osimertinib:** Leu, Val, Lys, Met, Ala, Gly, Glu, Cys, Asp.
		DMC	-7.6	0.686	
		Osimertinib	-7.6	1.751	
5D41	T790M V948R	ANP	-8.0	0.730	**DMC:** Glu, Leu, Phe, Met, Ile, Lys, Asp, Met. **Osimertinib:** Ile, Leu, Glu, Phe, Met, Lys, Asp.
		DMC	-7.1	0.992	
		Osimertinib	-6.1	0.937	
5UG8	T790M L858R V948R	8BP	-8.8	1.540	**DMC:** Phe, Leu, Val, Ala, Met, Arg. **Osimertinib:** Met, Leu, Val, Ala, Asn, Arg, Phe, Cys.
		DMC	-7.8	0.543	
		Osimertinib	-7.5	1.123	
5UG9	T790M L858R V948R	8AM	-9.1	1.427	**DMC:** Arg, Phe, Leu, Val, Ala, Met. **Osimertinib:** Val, Met, Ala, Leu, Phe, Glu, Cys.
		DMC	-7.7	0.543	
		Osimertinib	-8.0	1.755	
6LUD	T790M C797S L858R E865A E866A K867A	YY3	-7.3	1.622	**DMC:** Phe, Leu, Met, Val, Ala, Met. **Osimertinib:** Met, Gln, Ala, Leu, Ser, Gly, Val
		DMC	-7.2	0.942	
		Osimertinib	-7.8	1.053	

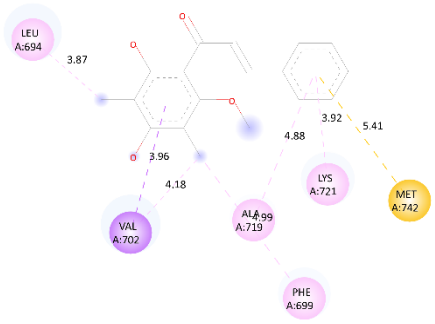

1M17 (DMC)

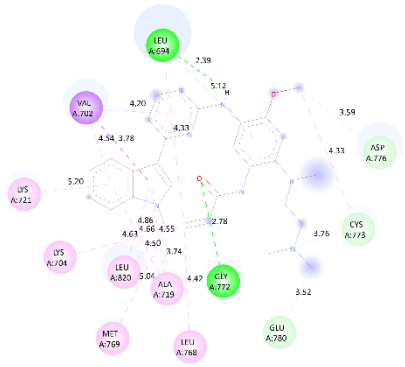

1M17 (Osimertinib)

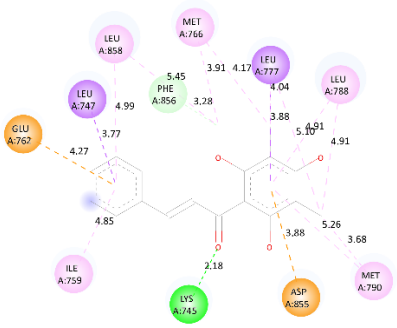

5D41 (DMC)

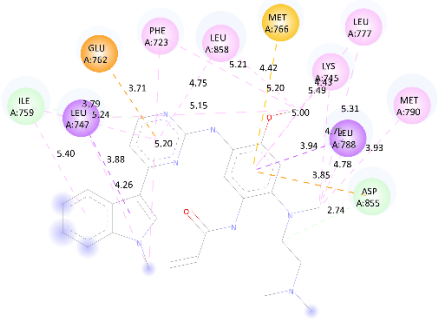

5D41 (Osimertinib)

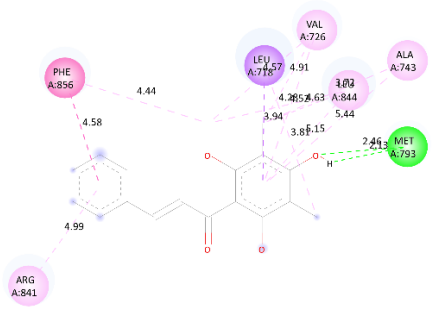

5UG8 (DMC)

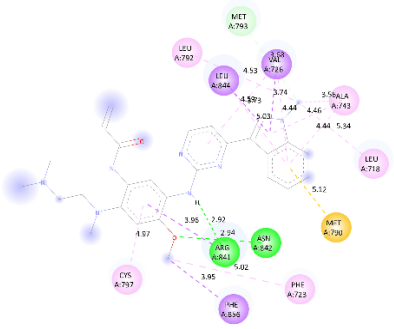

5UG8 (Osimertinib)

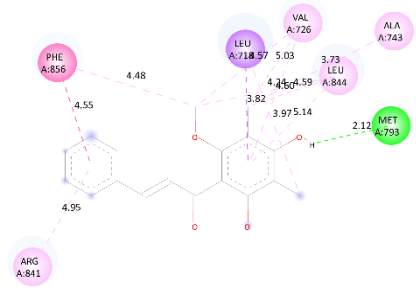

5UG9 (DMC)

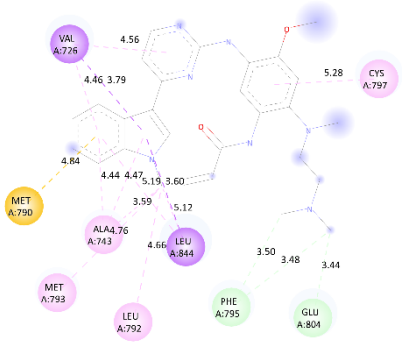

5UG9 (Osimertinib)

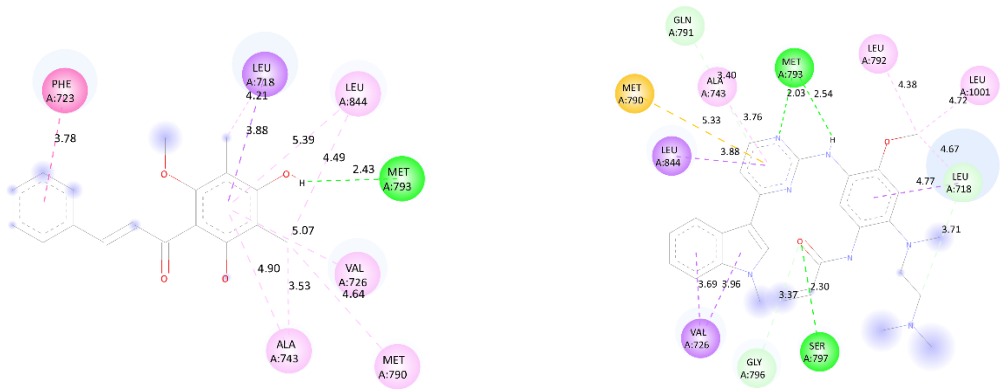

6LUD (DMC) 6LUD (Osimertinib)

Figure 5. Interaction of Ligands with Amino Acid Residues.

Docking analysis revealed that the DMC compound possesses a competitive affinity relative to osimertinib. A negative affinity value determines the level of protein-ligand stability; the more negative the value, the more stable the protein-ligand complex and the stronger or more spontaneous the interaction (Afriza et al. 2024). A lower RMSD value indicates a more stable bond position, which is considered valid if ≤ 2Å (Prasetiawati et al. 2021). The EGFR wild type (1M17) exhibits an affinity comparable to or greater than its natural ligand, reflecting its capability to bind competitively at the ATP-binding site.

DMC demonstrates a better binding affinity in the T790M/V948R (5D41) mutation. Threonine 790 acts as a gatekeeper residue, influencing the specificity of inhibitors in the ATP binding pocket. The T790M mutation leads to a narrowing of the ATP pocket, which increases ATP affinity and results in drug resistance, diminishing the effectiveness of inhibitors (Yun et al. 2008). It can maintain its binding with the critical residue Lys745 and form additional interactions with Asp855 and Glu762, leading to strong stabilization. In contrast, osimertinib relies more on hydrophobic interactions and loses direct contact with Lys745, which reduces its binding affinity (Tamirat et al. 2021). Therefore, it can be concluded that DMC has the potential to overcome the resistance caused by the T790M mutation, as it preserves critical interactions within the ATP-binding pocket.

Mutations in 5UG8 and 5UG9 occur in T790M, V948R, and L858R. The L858R mutation enhances the constitutive activity of EGFR, and its coexistence with T790M leads to a more complex resistance mechanism (Gomatou, Syrigos, and Kotteas 2023). DMC exhibits an affinity of –7.8 kcal/mol (5UG8) and –7.7 kcal/mol (5UG9), slightly better or nearly equivalent to osimertinib (–7.5 and –8.0 kcal/mol). The low RMSD of DMC (0.543 Å) indicates bond stability and demonstrates its potential in addressing this mutation combination (Prasetiawati et al. 2021).

Mutations in the 6LUD protein, specifically T790M, K867A, L858R, E865A, E866A, and C797S, signify advanced resistance to EGFR treatment. The C797S mutation notably diminishes the effectiveness of osimertinib due to its reliance on forming a covalent bond at Cys797 [21]. Docking studies indicate that osimertinib exhibits a better binding affinity (–7.8 kcal/mol) than DMC (–7.2 kcal/mol). Interaction analysis reveals that DMC forms hydrogen bonds with Met793 and establishes hydrophobic interactions with Leu718, Leu844, Val726, Ala743, and Met790. In contrast, osimertinib interacts with Met793, Ser797, and Gly796 but loses its covalent bond with Cys797 due to the mutation. This implies that while osimertinib retains a superior affinity, DMC may have the advantage of flexible non-covalent interactions that are not dependent on the Cys797 residue, potentially allowing it to remain effective in advanced resistance.

CONCLUSIONS

The compounds isolated using maceration, fractionation, and column chromatography methods were 2',4'-dihydroxy-6-methoxy-3',5'-dimethylchalcone (DMC) with MW: $C_{18}H_{18}O_4$ and lupeol with MW: $C_{30}H_{50}O$. The anticancer potential of DMC was simulated against the EGFR protein. The docking simulations revealed that DMC possesses potential as an alternative EGFR inhibitor, showing comparable or enhanced binding affinity relative to osimertinib in various mutations, particularly T790M and T790M/L858R/V948R, which are known to cause resistance to first- and second-generation inhibitors. The interaction pattern of DMC, which is dominated by hydrophobic residues, provides bond stability even without covalent bonds in Cys797, making it potentially more tolerant to the C797S mutation. Thus, DMC has the potential to be a promising non-covalent scaffold in overcoming EGFR resistance,

although validation through in vitro and in vivo tests is still needed.

Acknowledgements: The authors would like to thank all those who have contributed to this research, especially the Department of Chemistry, Andalas University, Indonesia.

Competing Interests: The authors declare that there are no competing interests.

REFERENCES

Abdullahi, R., Abubakar., & Mainul Haque. (2020). Preparation of Medicinal Plants: Basic Extraction and Fractionation Procedures for Experimental Purposes. *Journal of Pharmacy and Bioallied Sciences, 10(1),* 1-5. doi:10.4103/jpbs.JPBS_175_19

Afriza, D., Suriyah, W., Ichwan, S., & Knights, J., (2024). Molecular Docking Analysis between Anti-Apoptosis EGFR and Four Coumarins, and Four Carbazole Alkaloids: In Silico Study. *Padjadjaran Journal of Dentistry,* 36(1), 117. doi:10.24198/pjd.vol36no1.52467

Ahmad, S. (2022). Molecular Docking Simplified: Literature Review. *Advances in Medical, Dental and Health Sciences,* 4(4), 37–44. doi: 10.5530/amdhs.2021.4.8

Al-Temimi, Ali H.H., & Enas J.K. (2023). Determination and Isolation of Valuable Bioactive Compound (Lupeol) from *Portulacaria Afra* Jacq." *International Journal of Drug Delivery Technology,* 13(1), 199–204. doi:10.25258/ijddt.13.1.30

Aung, E.E., Kristanti A.N., Aminah. N. S., Takaya. Y., Ramadhan., & Aung, H, T. (2021). Anticancer Activity of Isolated Compounds from *Syzygium Aqueum* Stem Bark. *Rasayan Journal of Chemistry,* 14(1), 312–18. doi:0.31788/RJC.2021.1416106

Aung, E.E., Kristanti, A.N., Aminah, N.S., Takaya, Y., & Ramadhan, R. (2020). Plant Description, Phytochemical Constituents and Bioactivities of *Syzygium* Genus: A Review. *Open Chemistry,* 18(1), 1256–81. doi:10.1515/chem-2020-0175

Chandana, A. G., Suresha, B.S., Balasubramanian, T., & Ahalyadevi, K.H. (2024). *Syzigium Aqueum* : A Comprehensive Plant Review. *International Journal of Pharmacognosy*, JOTCSA,11(6), 255–61. doi:10.13040/IJPSR.0975-8232.IJP.11(6).255-61

Yulianti, H., Santoni, A., & Efdi, M. (2024). Isolation and Characterization of Cholest-5-En-3-Ol Compound from the Ethyl Acetate Extract of Stem Bark Ulin Plant (*Eusideroxylon zwageri Teijm & Binn*). 11(2), 919–24. doi: https://doi.org/10.18596/jotcsa.1379263

Ghafar, F., Nazri, T., Salleh, M., Hadi, N., Ahmad, N., Hamzah, A., Yusof, Z., & Azman, I. (2017). Total Phenolic Content And Total Flavonoid Content In *Moringa Oleifera* Seed. *Science Heritage Journal,* 1(1), 23–35. doi: 10.26480/gws.01.2017.23.35

Gomatou, G., Syrigos, N., & Kotteas, E. (2023). Osimertinib Resistance: Molecular Mechanisms and Emerging Treatment Options. *Cancers,* 15(3), 1–20. doi: 10.3390/cancers15030841

Habisukan, U.H., Elfita., Widjajanti, H., & Setiawan, A. (2021). Diversity of Endophytic Fungi in *Syzygium Aqueum*. *Biodiversitas*, 22(3), 1129–37. doi:10.13057/biodiv/d220307

Hadisaputri, Y.E., Cahyana, N., Muchtaridi., Lesmana, R., Rusdiana, T., Chaerunisa, A.Y., Sufiawati, I., Rostinawati, T., & Subarnas, A. (2020). Apoptosis-Mediated Antiproliferation of A549 Lung Cancer Cells Mediated by *Eugenia Aquea* Leaf Compound 2-,4-Dihydroxy-6-Methoxy-3-,5-Dimethylchalcone and Its Molecular Interaction with Caspase Receptor in Molecular Docking Simulation. *Oncology Letters,* 19(5), 3551–57. doi:10.3892/ol.2020.11466

Itam, A., Wati, M.S., Agustin, V., & Sabri, N. (2021). Comparative Study of Phytochemical, Antioxidant, and Cytotoxic Activities and Phenolic Content of *Syzygium Aqueum* (*Burm. f. Alston* f.) Extracts Growing in West Sumatera Indonesia." *Scientific World Journal*, 2021(3):1-9. doi:10.1155/2021/5537597

Jun, M., Fu, H.Y., Hong, J., Wan, X., Yang, C.S., & Ho, C (2003). Comparison of Antioxidant Activities of Isoflavones from Kudzu Root (Pueraria Lobata Ohwi). *Journal of Food Science,* 68(6), 2117-2122. https://doi.org/10.1111/j.1365-2621.2003.tb07029.x

Nopawit, K., Chaichuang, L., Rithchumpon, P., Phupong, P., Bhoopong, P., Tateing, S., Pompimon, W., Semakul, N., Chomsri, N., & Meepowpan, P. (2021). Synthesis, Cytotoxicity Evaluation and Molecular Docking Studies on 2′,4′-Dihydroxy-6′-Methoxy-3′,5′-Dimethylchalcone Derivatives. *RSC Advances,* 11(50), 31433–47. doi: https://doi.org/10.1039/D1RA05445G

Ishak, A.K.K, Aminah., & Yuliana, D. (2024). Literature Review : Uji Molekular Docking Senyawa Osimertinib Beserta Turunannya Terhadap Reseptor Tirosin Kinase Pada Kanker Paru-Paru. *Makassar Pharmaceutical Science Journal,* 2(1), 2024–65. doi: https://doi.org/10.33096/mpsj.v2i1.134

Lee, K.W., Kim, Y.J., Lee, H.J., & Lee, C.Y. (2003). Cocoa Has More Phenolic Phytochemicals and a Higher Antioxidant Capacity than Teas and Red Wine. *Journal of Agricultural and Food Chemistry.* 51(25), 7292–95. doi: 10.1021/jf0344385

Manaharan, T., Appleton, D., Cheng, H.M., & Palanisamy, U. (2012). Flavonoids Isolated from Syzygium Aqueum Leaf Extract as Potential Antihyperglycaemic Agents. *Food Chemistry,* 132(4), 1802–7. https://doi.org/10.1016/j.foodchem.2011.11.147

Mustarichie, R.., Runadi, D., & Danni, R. (2017). The Antioxidant Activity and Phytochemical Screening of Ethanol Extract, Fractions of Water, Ethyl Acetate, and n-Hexane from *Mistletoe Tea* (*Scurrula Atropurpurea* BL. Dans). *Asian Journal of Pharmaceutical and Clinical Research,* 10(2), 343-347. doi: 10.22159/ajpcr.2016.v10i2.15724

Hasnah, O., Rahim, A.A., Isa, N.M., & Bakhir, N.M. (2009). Antioxidant Activity and Phenolic Content of Paederia Foetida and Syzygium Aqueum. *Molecules,* 14(3), 970–78. doi: 10.3390/molecules14030970

Prasetiawati, R., Suherman, M., Permana, B., & Rahmawati. (2021). Molecular Docking Study of Anthocyanidin Compounds Against Epidermal Growth Factor Receptor (EGFR) as Anti-Lung Cancer. *Indonesian Journal of Pharmaceutical Science and Technology,* 8(1), 8-20. doi:https://jurnal.unpad.ac.id/ijpst/article/view/29872/15067

Rasyid, H., Purwono, B., & Pranowo, H.D. (2021). Design of New Quinazoline Derivative as EGFR (Epidermal Growth Factor Receptor) Inhibitor through Molecular Docking and Dynamics Simulation. *Indonesian Journal of Chemistry* 21(1): 201–11.

doi: https://garuda.kemdiktisaintek.go.id/documents/detail/2027377

Tamirat, M.Z., Kurppa, .J., Elenius, K., & Johnson, M.S. (2021). Structural Basis for the Functional Changes by EGFR Exon 20 Insertion Mutations. *Cancers,* 13(5), 1–21. doi: 10.3390/cancers13051120

Vachiraarunwong, A., Tuntiwechapikul, W., Wongnoppavich, A., Meepowpan, P., & Wongpoomchai, R. (2023). 2,4'-Dihydroxy-6'-Methoxy-3',5'-Dimethylchalcone from Cleistocalyx Nervosum Var. Paniala Seeds Attenuated the Early Stage of Diethylnitrosamine and 1,2-Dimethylhydrazine-Induced Colorectal Carcinogenesis. *Biomedicine and Pharmacotherapy,* 165, 115221. doi: https://doi.org/10.1016/j.biopha.2023.115221

Wang K, Yang JC, Jang YJ, Chen GY, Zhang YJ, Dai YH, Zhang DY, & Wu, YC. (2021). 19-(Benzyloxy)-19-Oxojolkinolide B (19-BJB), an Ent-Abietane Diterpene Diepoxide, Inhibits the Growth of Bladder Cancer T24 Cells through DNA Damage. *PLoS ONE,* 16, 1–24. doi:http://dx.doi.org/10.1371/journal.pone.0248468

Yun CH, Mengwasser KE, Toms AV, Woo MS, Greulich H, Wong KK, Meyerson M, Eck MJ. (2008). The T790M Mutation in EGFR Kinase Causes Drug Resistance by Increasing the Affinity for ATP. *Proceedings of the National Academy of Sciences of the United States of America,* 105(6), 2070–75. doi: 10.1073/pnas.0709662105

Zala, Shailesh P et al. (2012). Laboratory Techniques of Purification and Isolation. 4(June): 41–55.